Off-axis setup taking full advantage of incoherent illumination in coherence-controlled holographic microscope

Tomáš Slabý,[1,*] Pavel Kolman,[2] Zbyněk Dostál,[1,2] Martin Antoš,[1,2] Martin Lošťák,[1,2] and Radim Chmelík[1,2]

[1]*Institute of Physical Engineering, Faculty of Mechanical Engineering, Brno University of Technology, Technická 2, 616 69 Brno, Czech Republic*

[2]*CEITEC - Central European Institute of Technology, Brno University of Technology, Technická 10, 616 00 Brno, Czech Republic*

[*]*tomslaby@gmail.com*

Abstract: Coherence-controlled holographic microscope (CCHM) combines off-axis holography and an achromatic grating interferometer allowing for the use of light sources of arbitrary degree of temporal and spatial coherence. This results in coherence gating and strong suppression of coherent noise and parasitic interferences enabling CCHM to reach high phase measurement accuracy and imaging quality. The achievable lateral resolution reaches performance of conventional widefield microscopes, which allows resolving up to twice smaller details when compared to typical off-axis setups. Imaging characteristics can be controlled arbitrarily by coherence between two extremes: fully coherent holography and confocal-like incoherent holography. The basic setup parameters are derived and described in detail and experimental validations of imaging characteristics are demonstrated.

OCIS codes: (090.0090) Holography; (110.0113) Imaging through turbid media; (110.4980) Partial coherence in imaging; (120.5050) Phase measurement; (170.1790) Confocal microscopy; (180.3170) Interference microscopy.

References and links

1. R. Barer, "Interference microscopy and mass determination," Nature **169**(4296), 366–367 (1952).
2. H. G. Davies and M. H. F. Wilkins, "Interference microscopy and mass determination," Nature **169**(4300), 541 (1952).
3. H. Janečková, P. Veselý, and R. Chmelík, "Proving tumour cells by acute nutritional/energy deprivation as a survival threat: a task for microscopy," Anticancer Res. **29**(6), 2339–2345 (2009).
4. F. Dubois, C. Yourassowsky, O. Monnom, J. C. Legros, O. Debeir, P. Van Ham, R. Kiss, and C. Decaestecker, "Digital holographic microscopy for the three-dimensional dynamic analysis of in vitro cancer cell migration," J. Biomed. Opt. **11**(5), 054032 (2006).
5. E. Cuche, F. Bevilacqua, and C. Depeursinge, "Digital holography for quantitative phase-contrast imaging," Opt. Lett. **24**(5), 291–293 (1999).
6. L. Lovicar, L. Kvasnica, and R. Chmelík, "Surface observation and measurement by means of digital holographic microscope with arbitrary degree of coherence," Proc. SPIE **7141**, 71411S (2008).
7. L. Lovicar, J. Komrska, and R. Chmelík, "Quantitative-phase-contrast imaging of a two-level surface described as a 2D linear filtering process," Opt. Express **18**(20), 20585–20594 (2010).
8. T. Colomb, N. Pavillon, J. Kühn, E. Cuche, C. Depeursinge, and Y. Emery, "Extended depth-of-focus by digital holographic microscopy," Opt. Lett. **35**(11), 1840–1842 (2010).
9. F. Dubois, L. Joannes, and J.-C. Legros, "Improved three-dimensional imaging with a digital holography microscope with a source of partial spatial coherence," Appl. Opt. **38**(34), 7085–7094 (1999).
10. P. Klysubun and G. Indebetouw, "A posteriori processing of spatiotemporal digital microholograms," J. Opt. Soc. Am. A **18**(2), 326–331 (2001).
11. G. Indebetouw and P. Klysubun, "Optical sectioning with low coherence spatio-temporal holography," Opt. Commun. **172**(1-6), 25–29 (1999).
12. G. Indebetouw and P. Klysubun, "Imaging through scattering media with depth resolution by use of low-coherence gating in spatiotemporal digital holography," Opt. Lett. **25**(4), 212–214 (2000).
13. E. N. Leith, W.-C. Chien, K. D. Mills, B. D. Athey, and D. S. Dilworth, "Optical sectioning by holographic coherence imaging: a generalized analysis," J. Opt. Soc. Am. A **20**(2), 380–387 (2003).

#181222 - $15.00 USD Received 5 Dec 2012; revised 3 Feb 2013; accepted 2 May 2013; published 13 Jun 2013

14. M.-K. Kim, "Tomographic three-dimensional imaging of a biological specimen using wavelength-scanning digital interference holography," Opt. Express **7**(9), 305–310 (2000).
15. P. Massatsch, F. Charrière, E. Cuche, P. Marquet, and C. D. Depeursinge, "Time-domain optical coherence tomography with digital holographic microscopy," Appl. Opt. **44**(10), 1806–1812 (2005).
16. W. Choi, C. Fang-Yen, K. Badizadegan, S. Oh, N. Lue, R. R. Dasari, and M. S. Feld, "Tomographic phase microscopy," Nat. Methods **4**(9), 717–719 (2007).
17. T. Zhang and I. Yamaguchi, "Three-dimensional microscopy with phase-shifting digital holography," Opt. Lett. **23**(15), 1221–1223 (1998).
18. L. Xu, J. M. Miao, and A. Asundi, "Properties of digital holography based on in-line configuration," Opt. Eng. **39**(12), 3214–3219 (2000).
19. D. Carl, B. Kemper, G. Wernicke, and G. von Bally, "Parameter-optimized digital holographic microscope for high-resolution living-cell analysis," Appl. Opt. **43**(36), 6536–6544 (2004).
20. D. Shin, M. Daneshpanah, A. Anand, and B. Javidi, "Optofluidic system for three-dimensional sensing and identification of micro-organisms with digital holographic microscopy," Opt. Lett. **35**(23), 4066–4068 (2010).
21. P. Girshovitz and N. T. Shaked, "Generalized cell morphological parameters based on interferometric phase microscopy and their application to cell life cycle characterization," Biomed. Opt. Express **3**(8), 1757–1773 (2012).
22. B. Bhaduri, H. Pham, M. Mir, and G. Popescu, "Diffraction phase microscopy with white light," Opt. Lett. **37**(6), 1094–1096 (2012).
23. F. Dubois and C. Yourassowsky, "Full off-axis red-green-blue digital holographic microscope with LED illumination," Opt. Lett. **37**(12), 2190–2192 (2012).
24. R. Chmelík and Z. Harna, "Parallel-mode confocal microscope," Opt. Eng. **38**(10), 1635–1639 (1999).
25. R. Chmelík, "Three-dimensional scalar imaging in high-aperture low-coherence interference and holographic microscopes," J. Mod. Opt. **53**(18), 2673–2689 (2006).
26. H. Janečková, P. Kolman, P. Veselý, and R. Chmelík, "Digital holographic microscope with low spatial and temporal coherence of illumination," Proc. SPIE **7000**, 70002E (2008).
27. R. Chmelík and Z. Harna, "Surface profilometry by a parallel–mode confocal microscope," Opt. Eng. **41**(4), 744–745 (2002).
28. P. Kolman and R. Chmelík, "Coherence-controlled holographic microscope," Opt. Express **18**(21), 21990–22003 (2010).
29. M. Lošťák, P. Kolman, Z. Dostál, and R. Chmelík, "Diffuse light imaging with a coherence controlled holographic microscope," Proc. SPIE **7746**, 77461N (2010).
30. E. N. Leith and J. Upatnieks, "Holography with achromatic-fringe systems," J. Opt. Soc. Am. **57**(8), 975–980 (1967).
31. T. Slabý, M. Antoš, Z. Dostál, P. Kolman, and R. Chmelík, "Coherence-controlled holographic microscope," Proc. SPIE **7746**, 77461R (2010).
32. N. Pavillon, A. Benke, D. Boss, C. Moratal, J. Kühn, P. Jourdain, C. Depeursinge, P. J. Magistretti, and P. Marquet, "Cell morphology and intracellular ionic homeostasis explored with a multimodal approach combining epifluorescence and digital holographic microscopy," J Biophotonics **3**(7), 432–436 (2010).
33. B. Kemper, P. Langehanenberg, A. Höink, G. von Bally, F. Wottowah, S. Schinkinger, J. Guck, J. Käs, I. Bredebusch, J. Schnekenburger, and K. Schütze, "Monitoring of laser micromanipulated optically trapped cells by digital holographic microscopy," J Biophotonics **3**(7), 425–431 (2010).
34. E. Shaffer, N. Pavillon, and C. Depeursinge, "Single-shot, simultaneous incoherent and holographic microscopy," J. Microsc. **245**(1), 49–62 (2012).
35. M. Born and E. Wolf, *Principles of Optics*, 6th edition (Pergamon Press, 1986).
36. J. B. Pawley, *Handbook of Biological Confocal Microscopy* (Springer, 2006), pp. 65, Chap. 4.
37. N. Pavillon, C. S. Seelamantula, J. Kühn, M. Unser, and C. Depeursinge, "Suppression of the zero-order term in off-axis digital holography through nonlinear filtering," Appl. Opt. **48**(34), H186–H195 (2009).
38. T. Kreis, "Digital holographic interference-phase measurement using the Fourier-transform method," J. Opt. Soc. Am. A **3**(6), 847–855 (1986).
39. J. Kühn, F. Charrière, T. Colomb, E. Cuche, F. Montfort, Y. Emery, P. Marquet, and C. Depeursinge, "Axial sub-nanometer accuracy in digital holographic microscopy," Meas. Sci. Technol. **19**(7), 074007 (2008).
40. R. Chmelík, "Holographic confocal microscopy," Proc. SPIE **4356**, 118–123 (2001).
41. E. N. Leith and G. J. Swanson, "Recording of phase-amplitude images," Appl. Opt. **20**(17), 3081–3084 (1981).
42. R. Chmelík, P. Kolman, T. Slabý, M. Antoš, and Z. Dostál, "Interferometric system with spatial carrier frequency capable of imaging in polychromatic radiation," patent EP2378244B1 (July 4, 2012).

1. Introduction

Interference microscopes have become established instruments for measurements and study of microscopic samples and found many biological and industrial application areas. These instruments allow obtaining the amplitude and the phase of the wave reflected by or transmitted through the specimen. The reconstructed phase carries information about specimen topography or morphology and is therefore of particular interest. The quantitative phase contrast imaging allows non-invasive, marker-free (non-toxic) analysis of the specimen

#181222 - $15.00 USD Received 5 Dec 2012; revised 3 Feb 2013; accepted 2 May 2013; published 13 Jun 2013

with nanometer vertical resolution. In biological applications cell dynamics and morphology analyses can be performed such as monitoring of dry mass distribution within the cells [1–3] or cell tracking in 3D [4]. In technical applications topography measurements are most frequently performed [5–8]. Some interference microscope systems can also provide special features like numerical refocusing [9, 10], optical sectioning [11–13] or tomographic imaging [14–16].

Many interferometric instruments have been proposed for phase measurements, which can be basically classified into two groups. In-line systems [9, 17, 18] are characterized by the zero angle between the object and the reference beam. The use of low-coherence light sources in these systems enables to suppress coherent noise, but also to achieve an optical sectioning effect by coherence gating. However, these systems require capturing more than one interferogram to reconstruct the object wave, which can be a limiting factor when imaging rapidly varying phenomena. Also this is disadvantageous since vibrations and medium fluctuations can introduce measurement errors. On the other hand off-axis systems, frequently called as digital holographic microscopes (DHM) [5, 19–21], are characterized by the non-zero angle between the object and the reference beam. These systems do not allow the use of incoherent light sources and therefore the optical sectioning property is not available as well as the coherent noise suppression effect. Also the lateral resolution is limited due to this reason. However, only one captured interferogram is needed to reconstruct the object wave which makes these systems suitable for imaging of rapidly varying phenomena and brings high stability of the phase measurement.

The coherence-controlled holographic microscope (CCHM) combines an off-axis configuration and an achromatic grating interferometer allowing for the use of arbitrarily low-coherent illumination. This enables the CCHM to gain the described advantages of both in-line and off-axis systems while eliminating the disadvantages at the same time. Thus CCHM is capable to provide speckle-free real-time optically-sectioned quantitative phase contrast imaging with lateral resolution fully comparable to conventional optical microscopes. Recently some interesting off-axis setups emerged employing diffraction gratings and using sources of low temporal coherence [22, 23]. However, in [22] spatially coherent illumination is needed. In [23] spatial coherence is also increased to a certain extent.

To our knowledge, the first achromatic holographic microscope allowing for off-axis holographic imaging with light of arbitrarily low coherence was designed by Chmelík and Harna for reflected light [24]. The confocal-like optical sectioning property of CCHM systems was proved theoretically and experimentally for reflected-light configuration [24]. The theoretical description of the imaging process of CCHM was carried out and compared to other imaging systems [25]. Time-lapse analyses of living cells [3,26] and surface profilometry measurements [6,7,27] were made using the CCHM. A novel method of combined phase and depth-discriminated intensity imaging was proposed [6]. Recently some remarkable imaging properties of CCHM were discovered when imaging through scattering media [28, 29]. In 2010 the name “Coherence-controlled holographic microscope” was firstly introduced [28] as it reflects the crucial ability of the microscope to control its imaging properties by the degree of spatial and temporal coherence of the illuminating light. In this way imaging properties of the microscope can be easily adapted to match the application requirements.

The latest concept of the transmitted-light CCHM was described in detail and its optical properties were discussed in [28]. This device provided a remarkable progress in the CCHM design and created a platform for variety of mainly biological observations [3,26]. This concept employs a diffraction grating used as a beamsplitter to split the incident light into the object beam and the reference beam. Since the diffraction grating plane is optically conjugated with the output plane of the microscope as proposed by Leith [30], the formation of an achromatic interference fringe pattern in the output plane is ensured for arbitrarily low coherence of illumination. However, this design has some limiting factors. The most significant limitation is introduced to the spectral transmittance of the microscope for wavelengths different from central wavelength. This is the consequence of the dispersive

#181222 - $15.00 USD Received 5 Dec 2012; revised 3 Feb 2013; accepted 2 May 2013; published 13 Jun 2013

power of the diffraction grating, which produces laterally shifted images of the source in the entrance pupils of condensers. When using wavelengths longer or shorter than the central wavelength, the laterally shifted images of the source are cropped by the aperture of the entrance pupil which results in reducing the amount of interfering light while inducing increased spatial coherence of the source at the same time. Thus signal quality at these wavelengths is affected. This also causes slightly anisotropic transfer of spatial frequencies. Another important disadvantage of this concept is given by the need of four identical microscope objectives (two acting as condensers and two as objectives). Although long working distance lenses are employed, the lack of working space between condensers and objectives is significant especially when working with high NA lenses. The considerable limitation is also given by economical aspects when considering the costs of four identical objectives employed in the setup for each magnification.

The concern of this paper is to describe in detail the novel optical setup of the CCHM which we designed and which overcomes most of the mentioned disadvantages of the previous concept, preserves all the advantages of incoherent off-axis holography and enables multimodal imaging. Some of the preliminary results were already presented in [31]. In the following sections the basic setup parameters are derived and described in detail and experimental validations of imaging characteristics are demonstrated.

2. Optical setup and principles of operation

The novel CCHM setup (Fig. 1) is based on Mach-Zehnder-type interferometer adapted for achromatic off-axis holographic microscopy. The light passing through the achromatic interferometer propagates through separated optical paths – the object and the reference arm of the interferometer. Both arms are formed by identical microscope setups consisting of condensers (C_1, C_2), infinity-corrected objectives (O_1, O_2) and tube lenses (TL_1 TL_2). The essential component of the CCHM setup is the reflection diffraction grating (DG), which is placed in the reference arm of the interferometer and imaged into the output plane (OP) as proposed by Leith [30]. The diffraction grating plane (DG) and object planes (Sp, R) of objectives are optically conjugated with the output plane (OP) by objectives and output lenses (OL_1, OL_2). Since only the + 1st order of the diffraction grating is used for imaging (other diffraction orders are eliminated by spatial filtering in focal plane of output lens OL_2), the image of the grating is not formed directly by the reference beam in the output plane. However, when the object beam and the reference beam recombine in the output plane, the interference fringe pattern appears, which corresponds to the diffraction grating grooves' image as it would be formed directly by 0th and + 1st order of the diffraction grating. Thus the spatial frequency of interference fringes f_C in the output plane – i.e. the carrier frequency – equals to the spatial frequency of diffraction grating grooves f_G reduced by output lenses' magnification m_{OL}

$$f_C = \frac{f_G}{m_{OL}}. \tag{1}$$

#181222 - $15.00 USD Received 5 Dec 2012; revised 3 Feb 2013; accepted 2 May 2013; published 13 Jun 2013

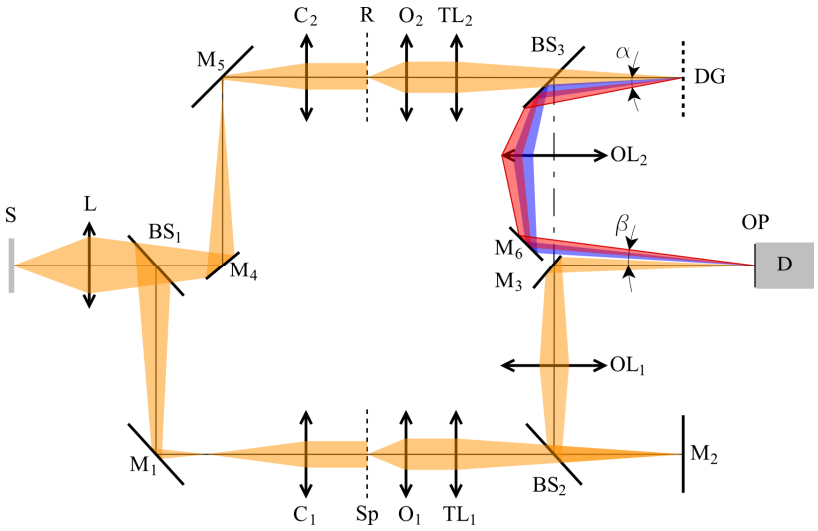

Fig. 1. Optical setup of the microscope. Light source (S), relay lens (L), beamsplitters (BS), mirrors (M), condensers (C), specimen plane (Sp), reference plane (R), microobjectives (O), tube lenses (TL), diffraction grating (DG), output lenses (OL), output plane (OP), detector (D).

The extended and broadband, i.e. spatially and temporally incoherent light source (S) (e.g. a halogen lamp) is imaged by a collector lens (L) to front focal planes of condensers, thus providing the Köhler illumination. Then the secondary image of the source is formed in the rear focal planes of objectives and also the tertiary image of the source is formed near the rear focal planes of output lenses. In the reference arm, the tertiary image of the source in the rear focal plane of the output lens OL_2 is spectrally dispersed with respect to the dispersive power of the diffraction grating so that the longer is the wavelength of light, the further the image of the source is placed from the reference arm axis. Let trace the axial ray which comes from the source, passes through the reference arm and hits the grating. When considering the + 1st diffraction order of the grating, the incident ray is diffracted by the grating at an angle α according to the grating equation $\sin(\alpha) = f_G\lambda$, where λ is the wavelength of light. The diffracted ray then passes through the output lens OL_2 and enters the output plane at an angle β. The relation between α and β is given by $\sin(\beta) = \sin(\alpha)/m_{OL}$. In the object arm of the interferometer, the light is reflected by mirror M_2 and passes through the output lens OL_1 normally since there is no diffractive element in the path. The light is not spectrally dispersed in this arm. Thus rays of different wavelengths emitted from corresponding points of tertiary images of the source in both interferometer arms recombine in the output plane under different angles β. This is caused by the dispersive power of the diffraction grating and gives rise to interference fringes parallel with grooves of the diffraction grating and of a spatial carrier frequency f_C which is constant for all wavelengths – i.e. the interferometer is achromatic. If a specimen (Sp) is observed, an image plane off-axis hologram with the spatial carrier frequency f_C is formed in the output plane.

A proper alignment of the output angle β for all available wavelengths is crucial for achromaticity of the interferometer. When any misalignment θ is introduced to the output angle β, the interferometer produces interference fringes of slightly different carrier frequencies at different wavelengths. The higher values of θ give rise to higher values of f_C and vice versa. Also the positive values of θ give rise to higher values of f_C at shorter wavelengths while the negative values of θ give rise to higher values of f_C at longer wavelengths. This behavior significantly influences achromaticity of the interferometer and consequently the contrast of the interference fringes pattern in the recorded hologram. Therefore the output angle β has to be properly aligned.

Although the use of incoherent illumination brings high demands on precise alignment of optical components, a simple and fully automatable two-step procedure was developed for

#181222 - $15.00 USD Received 5 Dec 2012; revised 3 Feb 2013; accepted 2 May 2013; published 13 Jun 2013

easy operation of the microscope. To equalize optical paths the mirror M_2 is shifted along the optical axis with the use of piezo-positioner. Second piezo-positioner is used to translate the reference objective O_2 perpendicularly to the optical axis to align precisely images from both interferometer arms formed in the output plane.

Several variations of the proposed setup are possible, e.g. with the use of transmission diffraction grating or with the use of two diffraction gratings, each placed in one arm of the interferometer. The use of transmission grating would be more convenient because of lower light losses, which are otherwise significant when considering the use of reflection diffraction grating together with beamsplitters (BS_2, BS_3). Also a reflected-light setup can be easily achieved by introducing illumination beams into the infinity space between objectives and tube lenses. In the same way, multimodality can be achieved by implementing other imaging or micromanipulation techniques to provide combined imaging [32–34].

The following components were used in our experimental setup: light source S (halogen lamp coupled into light guide), collector lens L (achromatic doublet, focal length 50 mm), condensers C (NA 0.52), objectives O (Nikon Plan Achromat 10 × /0.25, infinity-corrected), tube lenses TL (focal length 200 mm), output lenses OL (focal length 35 mm, NA 0.25, plan-corrected), detector D (CCD, BW, 14-bit, 1376 pixels × 1038 pixels, pixel size 6.45 μm). It is highly desirable to employ plan-corrected optics for the imaging part of the microscope setup (O, TL, OL) because of the detector D used as a recording device.

3. Incoherence of the light source

As it was already mentioned, the above described setup allows using illumination of arbitrary degree of coherence. Using of incoherent illumination in CCHM brings advantageous imaging properties and therefore the lowest achievable degree of coherence is of great importance. To demonstrate this achievable degree of coherence, one can estimate coherence width (CW) and coherence length (CL) of the illuminating light.

We estimated CW as a diameter of circular area that is illuminated almost coherently, which we expressed as the full width at half maximum (FWHM) d_w of the mutual intensity function. From the formula for this function [35, p. 511] it can be computed that $d_w = 0.7\,\lambda_0 / \gamma$, where λ_0 is central wavelength and γ is angular radius of the tertiary image of the light source as viewed from the output plane. According to [35, p. 319] the CL can be calculated as $d_l = \lambda_0^2 / \Delta\lambda_0$, where $\Delta\lambda_0$ is FWHM of the spectral function. For parameters of the real setup (γ ≈0.0063 rad, λ_0 ≈570 nm and $\Delta\lambda_0$ ≈150 nm) we obtained values of CW d_w ≈63 μm (calculated in the output plane) and CL d_l ≈2.2 μm. However, these values are only approximate and do not reflect the increase of coherence in tertiary images of the light source introduced by the imaging process when the light source is imaged by the optical system to focal planes of the output lenses.

To confront the theoretical values with real conditions and to measure the real values of CW and CL for our experimental setup an experiment was performed. A white (unfiltered) light illumination was provided by 5 mm diameter light source. Objective lenses 10 × /0.25 were used in this experiment.

To find the mutual intensity function a 2-axis piezo-positioner was used to translate the reference objective (O_2) in a direction perpendicular to the optical axis. Thus the image formed by the reference arm in the output plane was shifted with respect to the image formed by the object arm. The reference objective was translated in two directions – perpendicular to diffraction grating grooves (x axis) and parallel with diffraction grating grooves (y axis). The average values of the reconstructed amplitude were then computed in area of 5 px × 5 px within the central part of the image and the normalized values were plotted versus the lateral shift d_{OP} of the image formed by the reference arm in the output plane (Fig. 2(a)). The CW was estimated as the FWHM of the mutual intensity function, giving $d_{w,x}$ ≈91 μm and $d_{w,y}$ ≈76 μm for the two directions respectively.

Similar procedure was performed to measure the mutual coherence function and to find the CL. However, at this time 1-axis piezo-positioner was used to translate the mirror M_2. In

#181222 - $15.00 USD Received 5 Dec 2012; revised 3 Feb 2013; accepted 2 May 2013; published 13 Jun 2013

this way the optical path difference (OPD) between the two interferometer arms was varied. The averaged and normalized amplitude values versus the OPD value d_{OPD} were plotted and the CL was estimated as the FWHM of the obtained mutual coherence function giving $d_l \approx 4$ µm (Fig. 2(b)).

It can be seen that the experimentally determined values of CW and CL are higher when compared to the theoretical values. Partially it is an expected effect due to the increase of coherence by the imaging process as it was mentioned above. Moreover, the reference beam is spectrally dispersed when passing through the output lens contrary to the object beam. For this reason, small phase shifts introduced by residual aberrations of these lenses are not balanced in the output plane and individual interference patterns belonging to different wavelengths are unequally laterally shifted. The patterns belonging to different parts of the spectrum then match and thus contribute to the output signal for different values of the shifts d_{OP} (in x axis) and d_{OPD}, which is probably the reason for higher measured values of $d_{w,x}$ and d_l . This effect together with the presence of secondary maxima of the spectrum (caused by the reflection diffraction grating) may explain also the side-lobes of the curve in the Fig. 2(b).

The obtained values demonstrate the extremely low coherence of illumination which the CCHM is capable to utilize.

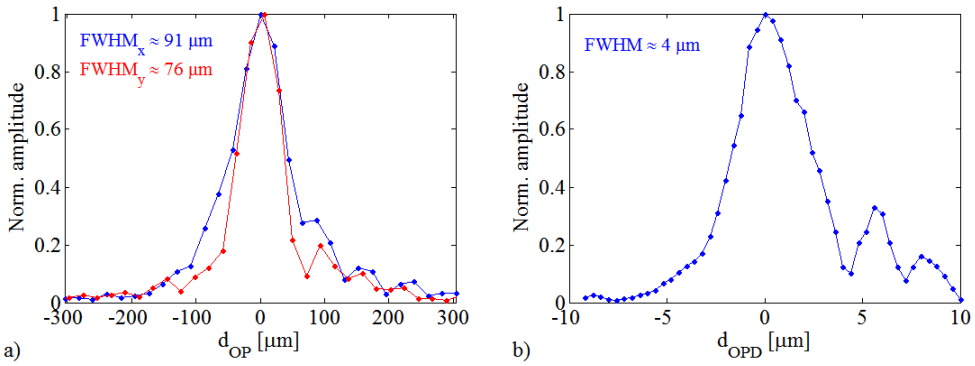

Fig. 2. (a) Normalized amplitude versus the lateral shift d_{OP} of the image formed by the reference arm in the output plane (measured in the output plane) in x and y axes and the corresponding FWHM values giving the estimation of CW. (b) Normalized amplitude versus optical path difference d_{OPD} and the corresponding FWHM value giving the estimation of CL.

4. Lateral resolution

Let the complex amplitude distribution of object and reference wave in the output plane be $o(x, y)$ and $r(x, y)$ respectively, where $r(x, y) = r_0(x, y)\exp(-i2\pi f_C x)$ and $r_0(x, y)$ is the complex amplitude distribution of reference wave expressed in the plane perpendicular to propagation direction. Then the intensity distribution of the hologram which is generated in the output plane by interference of the two waves is given by

$$\begin{aligned} i(x,y) &= \left|o(x,y)+r(x,y)\right|^2 = \\ &= \left|o\right|^2+\left|r\right|^2+or^*+o^*r = \\ &= \left|o\right|^2+\left|r\right|^2+or_0^*\exp(i2\pi f_C x)+o^*r_0\exp(-i2\pi f_C x), \end{aligned} \tag{2}$$

where asterisk denotes the complex conjugate operator and x, y are coordinates defined in the output plane. The first two terms in second row of Eq. (2) correspond to the intensities of object and reference waves, respectively. In the spatial frequency spectrum of hologram these terms create so-called zero-order term, or^* is the image term and o^*r is its complex conjugate, i.e. the twin image. Both the terms or^* and o^*r can be used for reconstruction of the object amplitude and phase (see section 7). In Fig. 3 the spatial-frequency spectrum

#181222 - $15.00 USD Received 5 Dec 2012; revised 3 Feb 2013; accepted 2 May 2013; published 13 Jun 2013

support (areas of non-zero values) of a hologram is depicted with all the terms of Eq. (2) for CCHM in comparison with a typical DHM setup. The form of the supports is explained in the following text. For purposes of the following paragraphs it should be noted that the Fourier transform of the terms $|o|^2$ and $|r|^2$ is the autocorrelation of the Fourier transform of o and r, respectively, and the Fourier transform of the term or^* is the convolution of the Fourier transform of o and r^* (and analogically for the term o^*r).

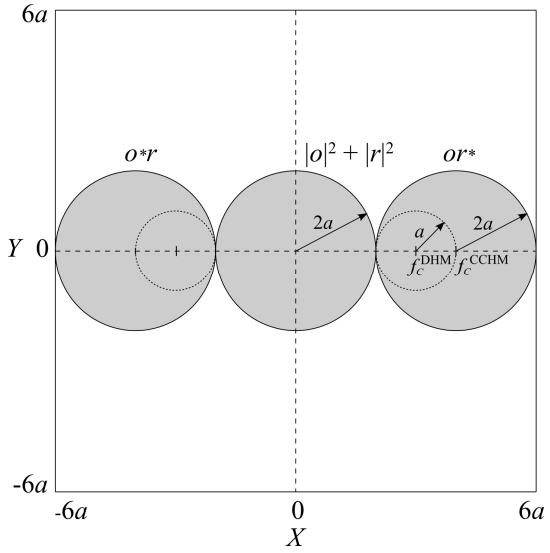

Fig. 3. Scheme of an ideal spatial-frequency spectrum support of a hologram captured by CCHM with spatially incoherent illumination (solid circles) and by a typical DHM setup using spatially coherent illumination (dashed circles).

The theoretical highest lateral frequency $f_{\max,o}$ carried by o is given by numerical aperture NA_O of the objective, total magnification m (between the output plane and the object plane of objectives) and wavelength of light λ as $f_{\max,o} = NA_O / (m\lambda)$. Then the spectral support of the term $|o|^2$ in the spatial frequency spectrum of a hologram is a circle of radius $2a$, where

$$2a = 2 f_{\max,o} = \frac{2NA_O}{m\lambda}. \tag{3}$$

Let us consider now two extreme cases of illumination: fully spatially coherent and fully spatially incoherent.

In typical off-axis DHM setups spatially coherent sources such as lasers or laser diodes are usually used to ensure the proper functionality of the device. Therefore the frequency spectrum of r_0 is nearly a two-dimensional Dirac distribution. Thus the highest frequency produced by the terms or_0^* and o^*r_0 in the spatial frequency spectrum is given by $f_{\max,or*}^{DHM} = f_{\max,o}$ and their spectral supports are therefore circles of radius

$$a = f_{\max,or*}^{DHM} = \frac{NA_O}{m\lambda} \tag{4}$$

(marked by dashed line in Fig. 3). It can be seen that the use of spatially coherent light sources in these systems leads to twice higher lateral resolution limit when compared to conventional optical microscopes where it is given by the standard formula $f_{\max}^{OM} = 2NA_O / (m\lambda)$ and where spatially low-coherent sources are used.

#181222 - $15.00 USD Received 5 Dec 2012; revised 3 Feb 2013; accepted 2 May 2013; published 13 Jun 2013

In the case of CCHM the use of spatially and temporally incoherent sources is allowed. Therefore an extended and broadband source can be employed, which provides a range of illumination directions in both interferometer arms. When a proper condenser is used so that the aperture of the objective is fully filled by the image of the source, then the highest spatial frequency of r_0 is given by $f_{\max,r}^{CCHM} = f_{\max,o}$. Thus the highest frequency produced by the terms or_0* and o*r_0 in the spatial frequency spectrum is given by $f_{\max,or*}^{CCHM} = 2 f_{\max,o}$ and their spectral supports are therefore circles of radius 2a, where

$$2a = f_{\max,or*}^{CCHM} = \frac{2NA_O}{m\lambda} \tag{5}$$

(marked by solid line in Fig. 3). It can be seen that the lateral resolution limit achievable by the CCHM with spatially incoherent illumination is fully comparable to conventional optical microscopes and it is half of the value for coherent illumination, the mode used in most current DHMs. Thus the lateral resolution limit of CCHM corresponds to incoherent imaging process [25]. Since the highly incoherent illumination as well as highly coherent is possible, the lateral resolution can be controlled arbitrarily in CCHM between the two extremes described by Eq. (4) and Eq. (5). Moreover due to the achromatic interferometer design of the CCHM, the wavelength of illuminating light can be varied arbitrarily (in the range of spectral transmissivity of the CCHM setup) to reach the best resolution achievable in the particular application.

To confront these theoretical conclusions with real imaging conditions and to prove the influence of spatially incoherent illumination on the achievable resolution in CCHM, we observed a sample with broad spectrum of spatial frequencies (surface of a ground glass). Multiple of captured holograms were averaged to increase SNR and preserve the highest spatial frequencies located near the resolution limit of the objective lens (10 × /0.25). Then the modulus of spatial-frequency spectrum of the averaged hologram was calculated (Fig. 4). The images were captured under two different conditions of illumination – highly spatially incoherent (halogen lamp coupled into 5 mm diameter light guide with interference filter λ = 650 nm, 10 nm FWHM) and highly spatially coherent (HeNe laser, λ = 633 nm). The spatially coherent illumination was provided to allow comparison of results obtained by CCHM in incoherent mode with those for a typical DHM (simulated by CCHM in coherent mode). The circles in Fig. 4 show the expected diameters of spectral supports of zero-order term and image terms corresponding to Eq. (5) and Eq. (4). Although one have to be cautious when directly comparing the diameters because of slightly different wavelengths used (650 nm vs. 633 nm), the experimental results show a good agreement with the theoretical assumptions. Also one can notice the different shapes of spatial frequency transmission profiles in the image terms, where the profile is approximately triangular for spatially incoherent illumination and rectangular for spatially coherent illumination. This is an important fact to understand the difference in the achievable lateral resolution between spatially incoherent and spatially coherent illumination. While spatially coherent illumination will provide good contrast even at the maximum transmitted spatial frequency, the spatially incoherent illumination will provide contrast approaching zero at its maximum transmitted spatial frequency. However, the maximum transmitted spatial frequency for spatially incoherent illumination will be double that of spatially coherent illumination.

#181222 - $15.00 USD Received 5 Dec 2012; revised 3 Feb 2013; accepted 2 May 2013; published 13 Jun 2013

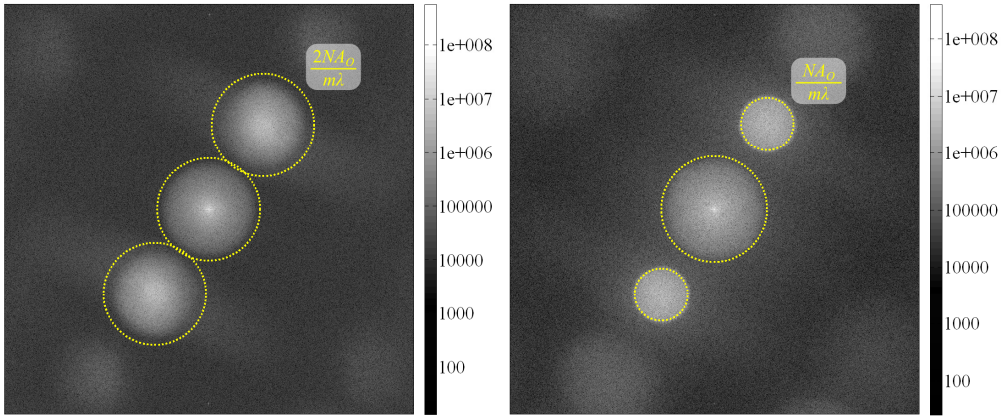

a) b)

Fig. 4. Modulus of spatial-frequency spectrum of a hologram (average of 30 images) captured by CCHM under condition of (a) spatially incoherent illumination (at 650 nm) and (b) spatially coherent illumination (at 633 nm). The circles show the expected diameters of spectral supports of zero-order term and image terms corresponding to Eq. (5) and Eq. (4). The amplitude values are in logarithmic scale (arbitrary units). Objectives used: 10 × /0.25.

5. Spatial frequency of the diffraction grating

Conditions derived in previous paragraphs are essential for determination of the diffraction grating spatial frequency. To perform a hologram reconstruction, total separation of the sideband terms or^* and o^*r from the zero-order term $|o|^2 + |r|^2$ is required in the spatial frequency spectrum as it is depicted in Fig. 3. No overlap of these terms is allowed. It can be seen from Fig. 3 that the carrier frequency is then given as $f_C^{DHM} \geq 3a$ in the case of DHM and $f_C^{CCHM} \geq 4a$ in the case of CCHM. The need of higher carrier frequency in the case of CCHM is the consequence of higher lateral resolution. This influences negatively the available field of view (FOV) as it will be discussed in the next section. The total magnification m between the output plane and the object plane of objectives O_1, O_2 is given as $m = m_O m_{OL}$, where m_O is magnification of objectives and m_{OL} is magnification of output lenses. The condition for carrier frequency in the output plane of the CCHM is thus given by

$$f_C^{CCHM} \geq 4a = \frac{4NA_O}{m_O m_{OL} \lambda}. \tag{6}$$

When considering Eq. (1) we obtain a condition for diffraction grating grooves' spatial frequency in the form

$$f_G \geq \frac{4NA_O}{m_O \lambda}. \tag{7}$$

The spatial frequency of the diffraction grating used in our setup is $f_G = 150$ mm^{-1}, which is designed for $\lambda = 650$ nm and $NA_O/m_O \leq 0.025$ ratio. When a shorter wavelength or objectives with higher NA_O/m_O ratio are to be used, then higher values of f_G are required to avoid an overlap of the sideband terms and the zero-order term in the spatial frequency spectrum (e.g. $f_G = 222$ mm^{-1} is required for $\lambda = 450$ nm and $NA_O/m_O = 0.025$).

6. Output lens and the field of view

Output lenses are used in the CCHM setup to relay the images of the object planes (Sp, R) and the diffraction grating plane (DG) into the output plane (OP) of the interferometer. The second important role of output lenses is to ensure proper sampling of the hologram by a detector. Magnification m_{OL} of output lenses is dependent on the maximum spatial frequency

#181222 - $15.00 USD Received 5 Dec 2012; revised 3 Feb 2013; accepted 2 May 2013; published 13 Jun 2013

$f_{OP,\max}$ present in the hologram at the output plane that has to be resolved and recorded digitally. Taking into account the rotation of the detector by 45° around the optical axis with respect to interference fringes, this frequency can be derived as

$$f_{OP,\max} = \frac{\sqrt{2}}{2} f_C + f_{\max,or*} = (\sqrt{2}+1)\frac{2NA_O}{m_O m_{OL}\lambda}. \quad (8)$$

Since the sampling rate should be at least 2.3 times higher [36] a condition for the spatial frequency f_{CCD} (pixel density) of a CCD detector is given by

$$f_{CCD} \geq 2.3 f_{OP,\max}, \quad (9)$$

which in terms of Eq. (7) and Eq. (8) leads to

$$m_{OL} \geq 2.78 \frac{f_G}{f_{CCD}}. \quad (10)$$

For f_G = 150 mm^{-1} and a camera pixel size of 6.45 μm Eq. (10) gives $m_{OL} \geq 2.7$. The higher is f_G, the finer is the interference structure in the output plane and the larger magnification is thus needed to resolve the fringes by a detector and consequently the smaller is the field of view. Therefore it is convenient to keep f_G as low as possible. When compared to typical DHM, the resulting FOV is smaller in the case of CCHM due to higher lateral resolution (FOV dimensions are approximately 1.5 × smaller). However, CCHM offers a better (lower) resolution/FOV ratio (when preservation of NA_O/m_O ratio is assumed). This means that if objective lenses with higher NA_O (and corresponding m_O) would be used in DHM providing comparable resolution to CCHM, it would result in smaller FOV dimensions in the case of DHM. From another view, if objective lenses with lower magnification m_O (and corresponding NA_O) would be used in CCHM to provide comparable FOV as in DHM, it would result in worse achievable lateral resolution in the case of DHM. Also there is a difference in achievable extremes: objective lenses with highest available NA_O or lowest available magnification m_O. With the highest available NA_O objective lens the CCHM is able to provide better resolution when compared to DHM with the same lens, while with the lowest available magnification lens the DHM is able to provide larger FOV when compared to CCHM with the same lens. To extend the available FOV a larger detector with increased number of pixels can be used. There are also several methods enabling suppression of the zero order term in the frequency spectrum to improve the available bandwidth for the sideband terms (e.g [37].). In this way a lower magnification of output lenses is needed because of lower carrier frequency, which results in larger FOV dimensions. However, these methods are still more or less approximated.

There are also several more parameters of the output lenses that should be taken into account such as numerical aperture, lateral resolution or accessibility of the back focal plane. A stronger limiting condition for numerical aperture is given in the reference arm where the reference beam is deflected by the diffraction grating and has to be collected by the output lens OL_2. The lateral resolution has to be sufficient across the whole FOV to transfer all the spatial frequencies produced by objectives into the output plane. The accessibility of the back focal plane is important to enable elimination of all diffraction grating orders except the imaging order (l = + 1) by spatial filtering.

7. Image processing

The reconstruction of the image amplitude and phase from a captured hologram is based on carrier removal in the Fourier plane [24,38]. The hologram is Fourier transformed using the 2D fast Fourier transform (FFT) algorithm. Then the image spectrum in the sideband is extracted by a windowing operation. The window is centered at the carrier frequency f_C and the size of the window corresponds to the maximum image term spatial frequency $f_{\max,or*}$. The

#181222 - $15.00 USD Received 5 Dec 2012; revised 3 Feb 2013; accepted 2 May 2013; published 13 Jun 2013

frequency origin is translated to the center of the window and the spectrum is multiplied by an apodization function. Finally, the image complex amplitude is computed using the 2D inverse FFT and the image amplitude and phase are derived from the complex amplitude as modulus and argument, respectively.

8. Phase measurement accuracy and precision

There are several parameters that can influence the accuracy and/or precision of reconstructed phase in holographic microscopy such as coherent noise, parasitic interferences, shot noise, readout noise, quantization noise, wavelength stability, air flow, temperature fluctuations, mechanical robustness, numerical reconstruction algorithm etc. Thanks to the temporally incoherent light source CCHM enables strong suppression of coherent noise and parasitic interferences. This brings high quality and accuracy of the phase measurement. The sensitivity for wavelength stability issues is reduced thanks to the achromatic interferometer configuration. On the other hand the spatial incoherence of the light source causes decrease of interference fringes' contrast in the output plane. However, this can be easily overcome by the use of detector with increased bit depth.

To estimate the phase measurement precision we followed an approach described e.g. in [39]. The temporal standard deviation σ was computed for each pixel of the blank reconstructed phase image throughout the 15 s long sequence of 140 captured images (no averaging used). In this way maps of temporal standard deviations of reconstructed phase were calculated providing information on the precision achieved in any particular pixel of the reconstructed image (Fig. 5). The measurement was performed with 14-bit camera 1376 pixels × 1038 pixels under two different degrees of temporal coherence of illumination – halogen lamp filtered with interference filter (λ = 550 nm, 10 nm FWHM) and unfiltered (white light). Examples of central parts of captured holograms are shown in Fig. 5(a, b). With filtered light the interference fringes utilize 62% of dynamic range of the detector, while with white light the interference fringes utilize 28%. This gives 2.2 × lower contrast for white light when compared to filtered light. The obtained values of temporal standard deviations are in range of 0.002-0.006 rad for filtered light with mode of $\hat{\sigma}_{\varphi} = 0.003$ rad and 0.005-0.015 rad for white light with mode of $\hat{\sigma}_{\varphi} = 0.0085$ rad. Higher values of σ in the case of white-light illumination are probably caused by imperfect alignment of the output angle β, which influences achromaticity of the interferometer (see section 2) and decreases contrast of interference fringes. Higher values of σ at the edges of FOV are caused by slight decrease of interference fringes' contrast in these areas, which is a consequence of spatially incoherent illumination [28]. When assuming the difference of refractive indices between sample and surrounding environment Δn = 0.5, one can obtain temporal standard deviation values converted to a real height: $\hat{\sigma}_h = 0.5$ nm for filtered light illumination and $\hat{\sigma}_h = 1.5$ nm for white light illumination. In such case the phase-measurement precision effectively reaches a sub-nanometer regime with filtered light illumination. Since these results were achieved with experimental setup built on optical table, we suppose there is a space for improvement in alignment and mechanical and thermal stability to further refine the phase measurement precision. Also there is the possibility of frame averaging to achieve better precision values.

#181222 - $15.00 USD Received 5 Dec 2012; revised 3 Feb 2013; accepted 2 May 2013; published 13 Jun 2013

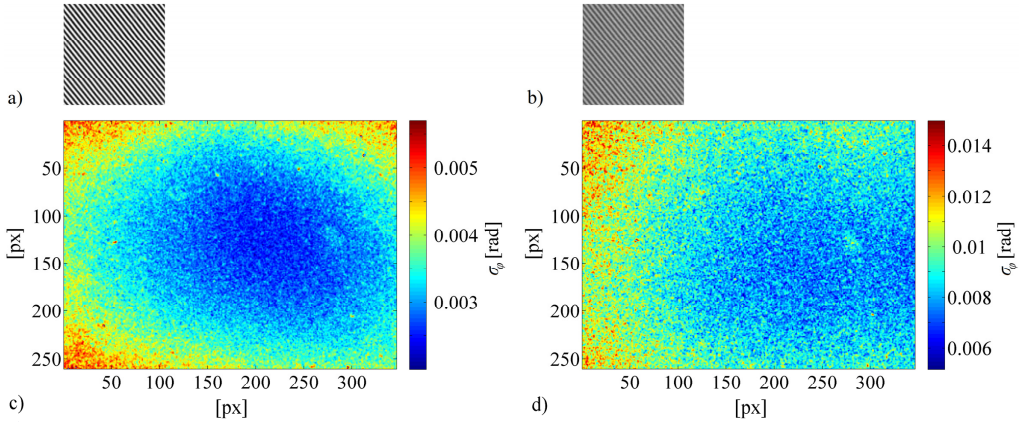

Fig. 5. Central parts of holograms (100 px × 100 px) captured with (a) filtered light (550 nm, $\Delta\lambda$ = 10 nm), (b) white light (unfiltered). For purpose of this publication, contrast in (a) and (b) was increased while maintaining contrast ratio between (a) and (b). Standard deviations σ_φ calculated for each pixel of the reconstructed phase image through 15 s long sequence of captured images with (c) filtered light (550 nm, $\Delta\lambda$ = 10 nm), (d) white light (unfiltered). Objectives used: 10 × /0.25.

9. Coherence gating

Thanks to the spatially and temporally incoherent illumination, the CCHM is capable of coherence gating, i.e. a limited contribution of light scattered in out-of-focus planes of the specimen to the resulting image. Low spatial coherence suppresses influence of scattered light in such a way that it limits interference of low-coherence non-ballistic photons. Temporal incoherence is transformed by the diffraction grating into spatial incoherence; broad-spectrum source then causes a similar effect of coherence gating as a spatially incoherent monochromatic source [28]. Limiting both spatial and temporal coherence in CCHM thus results in improved in-focus image contrast especially for objects embedded in a scattering media. In the case of reflected-light CCHM, true confocal-like optical sectioning by coherence gating is achieved [6, 24, 25].

To prove the coherence gating effect induced by incoherent illumination and the possibility of imaging through a scattering media in our transmitted-light setup, we observed amplitude object hidden behind a strong diffuser (D) – coverslip ground glass (Fig. 6(a)). In the object arm of the CCHM the diffuser placed in the out-of-focus plane spreads the image of the object in many directions. The reference arm then acts as a filter separating always a single image from the object arm image plane, where images spread one over each other are located because of scattering by the diffuser. In this way only the separated image contribute to the interference structure of the resulting hologram. Although the reference arm is usually adjusted to separate ballistic light (providing highest contrast of interference fringes), the diffuse light imaging is also possible with CCHM [29]. It can be seen in Fig. 6 that the structure of the specimen in the case of conventional bright-field image (Fig. 6(b)) is completely undistinguishable due to the diffused light, while the reconstructed CCHM amplitude (Fig. 6(c)) and phase (Fig. 6(d)) images still clearly reveal the structure. Although the interference signal is weak in case of such a strong diffuser, it still enables CCHM to acquire high-quality images of objects hidden behind it. However, this is only possible when the diffuser is located in the out-of-focus plane, otherwise the structure of the diffuser would affect the reconstructed image of the observed specimen.

#181222 - $15.00 USD Received 5 Dec 2012; revised 3 Feb 2013; accepted 2 May 2013; published 13 Jun 2013

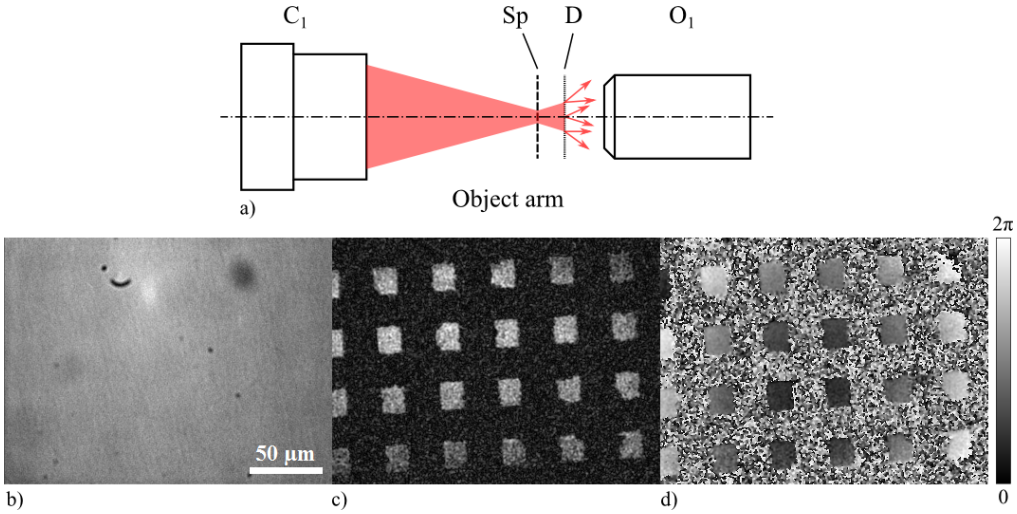

Fig. 6. Observation of an amplitude object hidden behind a strong diffuser. (a) Illustration of the object arm with inserted diffuser (D), (b) conventional bright-field image (captured with shutter closed in the reference arm), (c) reconstructed amplitude, (d) reconstructed phase. The amplitude and phase were reconstructed using a single hologram (no averaging). Objectives used: 10 × /0.25, interference filter λ = 650 nm, 10 nm FWHM.

10. Influence of spatial and temporal coherence on the imaging properties

Imaging properties of the CCHM can be varied to match the requirements of any particular application. This is done by controlling the degree of spatial and temporal coherence of the illuminating light. The degree of spatial coherence is controlled by an aperture diaphragm changing the effective area of the extended light source. The degree of temporal coherence is controlled by the use of bandpass filters together with white light source (e.g. halogen lamp). Higher degree of coherence allows for wider range of numerical refocusing. Lower degree of coherence results in several advantageous imaging properties. Reduction of spatial coherence brings better lateral resolution (see section 4). Reduction of both, spatial and temporal coherence, allows for coherence gating [25, 27, 28, 40], i.e. imaging through scattering media and confocal-like optical sectioning in the case of reflected-light setup. Also strong suppression of coherent noise and parasitic interferences is achieved in this way [41], resulting in high phase measurement accuracy and high imaging quality (Fig. 7, Fig. 8). When working in reflected-light mode, controlling the degree of coherence between coherent and incoherent mode enables a novel method of combined phase and depth-discriminated intensity imaging which overcomes the known 2π phase ambiguity [6]. In this way rough surfaces can be measured with nanometer precision. In addition to these features, achromatic off-axis geometry of CCHM allows for adaptation of illumination wavelength to take into account the spectral sensitivity of the specimen, spectral sensitivity of the detector or spectral output power of the light source. Also achievable lateral resolution and phase measurement precision can be varied in this way to optimize imaging performance in particular application. Composite color images of a sample can be obtained if a color camera is employed or by combining separate RGB intensity images.

#181222 - $15.00 USD Received 5 Dec 2012; revised 3 Feb 2013; accepted 2 May 2013; published 13 Jun 2013

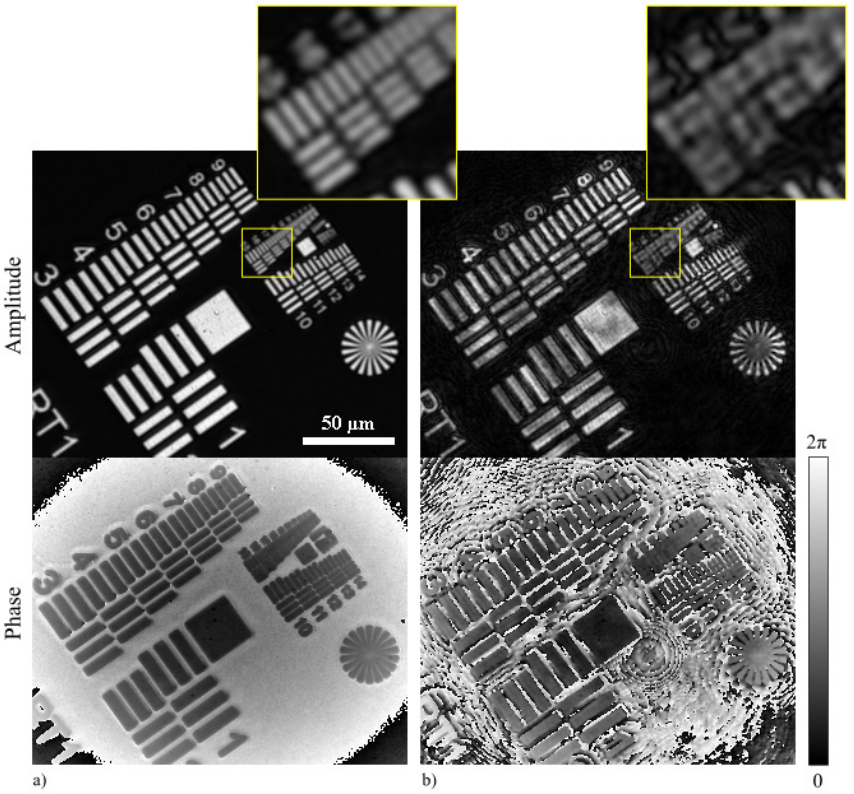

Fig. 7. Demonstration of imaging quality when observing a resolution target in (a) spatially and temporally low-coherent illumination (halogen lamp coupled into 5 mm diameter light guide with interference filter λ = 650 nm, 10 nm FWHM), (b) spatially and temporally coherent illumination (HeNe laser, 633 nm). Reduction of coherent noise and parasitic interferences is well demonstrated in the case of incoherent illumination as well as higher achieved lateral resolution (although it cannot be directly compared due to slightly different wavelengths used). Objectives used: 10 × /0.25.

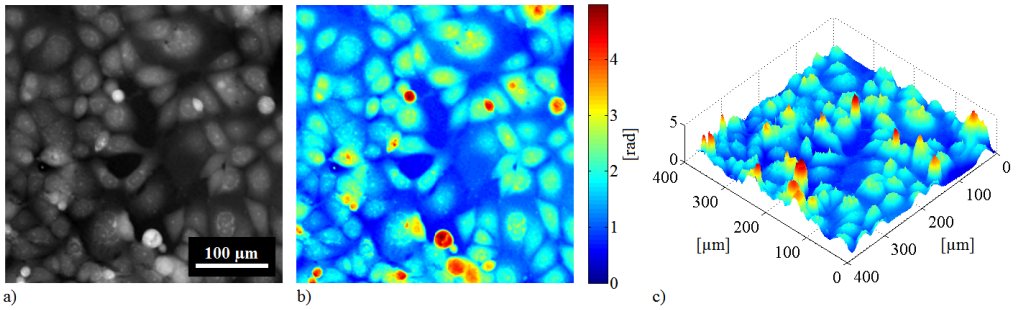

Fig. 8. Phase images of well spread cells of human breast adenocarcinoma cell line MCF-7 growing in vitro in eutrophic conditions. (a) Unwrapped phase image, (b) pseudo-color representation of unwrapped phase, (c) pseudo-color 3D representation of unwrapped phase. Images captured by CCHM at 650 nm (10 nm FWHM) with 10 × /0.25 objectives.

11. Conclusions

The proposed setup of CCHM enables off-axis holographic microscopy with completely temporally and spatially incoherent (i.e. broadband and extended) light sources. The degree of coherence influences strongly the imaging characteristics of CCHM, thus controlling the

#181222 - $15.00 USD Received 5 Dec 2012; revised 3 Feb 2013; accepted 2 May 2013; published 13 Jun 2013

degree of coherence brings the possibility to adapt the imaging characteristics according to particular application requirements. The main optical parameters were derived. Lateral resolution limit fully comparable to conventional widefield optical microscopes and twice smaller when compared to typical DHMs was demonstrated with spatially incoherent illumination. Also the phase measurement precision reaching a sub-nanometer regime was demonstrated. Coherence gating effect was proved when imaging an amplitude object hidden behind a strong diffuser. The influence of spatial and temporal coherence on the imaging properties was discussed pointing out the benefits of incoherent off-axis holography and the high imaging quality was presented.

The imaging characteristics of CCHM in coherent mode are comparable to typical DHM setups including the possibility to refocus numerically. In incoherent mode the CCHM is capable to provide high-quality speckle-free coherence-gated quantitative phase contrast imaging with sub-nanometer phase measurement precision and lateral resolution fully comparable to conventional optical microscopes. On the other hand these benefits of incoherent off-axis holography are at the price of more complex optical design. When compared to typical DHM setups, the CCHM provides better (lower) resolution/FOV ratio. Moreover the achromatic geometry of CCHM allows the illuminating wavelength to be chosen arbitrarily according to any requirement of any particular application or to optimize the imaging characteristics such as lateral resolution or phase measurement precision. It should be also noted that there is a limitation common for all off-axis geometry setups (including CCHM), which is the impossibility to fully exploit the available spatial frequency bandwidth of the detector. However, this limitation is balanced by the one-shot real-time measurement capability, which is the domain of off-axis systems.

When compared to previous generation of CCHM [28], the newly proposed setup eliminates spatial coherence limitation at wavelengths different from the central wavelength thus enabling the use of fully spatially incoherent sources at arbitrary wavelength of the visible spectrum. The number of required objective lenses was reduced from four to two and standard condensers are used with no need for replacement when magnification is changed. The working space and spectral transmittance were substantially improved to levels fully comparable with conventional optical microscopes.

By introducing the illumination beams into infinity spaces between objectives and tube lenses, the proposed setup can be easily adapted for reflected-light mode. Also multimodality can be achieved by implementing other imaging or micromanipulation techniques enabling CCHM to profit from combined holographic imaging.

Thanks to the real-time, non-invasive and marker-free imaging character, the CCHM in transmitted-light mode is very convenient for imaging of living cells [3,26]. In such applications imaging through scattering media is highly desirable feature of CCHM, which is enabled by the use of incoherent illumination. The CCHM in reflected-light mode is most frequently used for surface profiling [6,7,27], where the incoherent illumination enables a novel combined phase and depth-discriminated intensity imaging to overcome the 2π phase ambiguity [6].

The proposed CCHM technology is patented by Brno University of Technology [42].

Acknowledgments

The authors thank to colleagues from Experimental biophotonics group (CEITEC) for helpful discussions, especially to Michala Henzlová and Matěj Týč. This work was supported by Technology Agency of the Czech Republic (TE01020229), Ministry of Industry and Trade of the Czech Republic (FR-TI4/660) and CEITEC – Central European Institute of Technology (CZ.1.05/1.1.00/02.0068) from European Regional Development Fund.